Supplemental Material

Ab initio Determination of Ultrahigh Thermal Conductivity in Ternary Compounds

Huan Wu, Hang Fan, Yongjie Hu*

School of Engineering and Applied Science,

University of California, Los Angeles (UCLA), Los Angeles, CA, 90095

*Corresponding author. Email: yhu@seas.ucla.edu

S1. Details of the calculation and settings

The IFCs are derived through the following procedures. First, an irreducible displacement set is generated based on a real space supercell. For each displacement configuration, the Hellmann-Feynman forces on atoms were calculated by density functional theory using Quantum ESPRESSO package [1,2]. Then the IFCs are extracted by fitting the prepared displacement-force sets using the ALAMODE package [3]. We used projector-augmented wave pseudopotentials under local density approximation for density functional theory calculations [4]. The convergence threshold for self-consistency is 10^{-11}. The kinetic energy cutoff for electronic wavefunctions is 120 Ry for *R*3*m*-BNC_2, 80 Ry for *Pmm*2-BNC_2 and $P\bar{4}m2$-BNC_2, 100 Ry for BPC_2 and $BAsC_2$, and 120 Ry for BAs and Si, respectively. The primitive cell

of all the calculated BXC$_2$ has four atoms. The Monkhorst-Pack grids for structure optimization on primitive cells are $12 \times 12 \times 12$ for BNC_2, $18 \times 18 \times 18$ for BPC_2 and $BAsC_2$, and $6 \times 6 \times 6$ for BAs and Si, respectively. All the parameters for the density functional theory calculations has been carefully checked to make the uncertainty of the forces acting on each atoms less than 10^{-6} Ry/au.

The convergence of thermal conductivity versus all the setting parameters, including the cutoff radius for 3rd and 4th order IFCs, supercell size, and $\boldsymbol{q}$-mesh has been carefully checked and verified. For $Pmm2$ and $P\bar{4}m2$ phase ternary boron compounds, the 2nd-order IFCs are calculated based on a 256 atoms supercell, and the 3rd-order IFCs are calculated based on a 108 atoms supercell. For $R3m$ phase ternary boron compounds, the 2nd-order IFCs are calculated based on a 192 atoms supercell, and the 3rd-order IFCs are calculated based on a 108 atoms supercell. For BAs and Si, the IFCs are calculated based on a 216 atoms supercell. The Monkhorst-Pack grids for supercells are $4 \times 4 \times 4$ for BNC_2, $6 \times 6 \times 6$ for BPC_2 and $BAsC_2$, and $2 \times 2 \times 2$ for BAs and Si, respectively. The cut-off radius for 3rd-order IFCs are 6.8 bohr for ternary boron compounds. The cut-off radius for 4th-order IFCs is 3.0 bohr for $Pmm2$-BNC_2 and 4.7 bohr for $R3m$-BNC_2, respectively. For BAs, the 3rd-order and 4th-order IFCs include up to fifth nearest neighboring atoms and second nearest neighboring atoms, respectively. For Si, the 3rd-order IFCs include up to fifth nearest neighboring. The dipole-dipole interaction is considered by adding a non-analytical term to the dynamical matrix [5]. A tetrahedron method is applied here for the integration over Brillouin Zone [6], which makes the $\boldsymbol{q}$-mesh for solving the Boltzmann transport equation converged at a relatively small mesh density compared with smearing method. The $\boldsymbol{q}$-mesh for solving the Boltzmann transport equation is $12 \times 12 \times 12$ for $R3m$-BNC_2, $8 \times 8 \times 8$ for $Pmm2$-BNC_2, $12 \times 12 \times 12$ for $P\bar{4}m2$-BNC_2, $14 \times 14 \times 14$ for BPC_2 and $BAsC_2$ and $18 \times 18 \times 18$ for BAs.

S2. Theoretical details and solution of phonon Boltzmann equation with three-phonon and four-phonon scatterings

The phonon Boltzmann transport equation is given as,

$$\boldsymbol{v}_\lambda \cdot \nabla T \frac{\partial n_\lambda}{\partial T} = \left(\frac{\partial n_\lambda}{\partial t}\right)_{scattering} \qquad (S1)$$

where $\lambda \equiv (\boldsymbol{q}, p)$ labels a phonon mode with wave vector $\boldsymbol{q}$ and polarization p. $\boldsymbol{v}_\lambda$ is the group velocity of phonon mode λ, and n_λ is the non-equilibrium phonon distribution function. The scattering term $\left(\frac{\partial n_\lambda}{\partial t}\right)_{scattering}$ describes the change rate of n_λ due to phonon scatterings, and can be treated as the summation of different phonon scattering processes,

$$\left(\frac{\partial n_\lambda}{\partial t}\right)_{scattering} = \left(\frac{\partial n_\lambda}{\partial t}\right)_{3ph} + \left(\frac{\partial n_\lambda}{\partial t}\right)_{4ph} \qquad (S2)$$

$\left(\frac{\partial n_\lambda}{\partial t}\right)_{3ph}$ and $\left(\frac{\partial n_\lambda}{\partial t}\right)_{4ph}$ represent the change rate of n_λ due to three-phonon and four-phonon scatterings respectively. In our calculation, we noticed that considering four-phonon scatterings dramatically increases the computational cost. Based on Fermi's golden rule [7],

$$\begin{aligned}\left(\frac{\partial n_\lambda}{\partial t}\right)_{3ph} = \frac{2\pi}{\hbar^2}\sum_{\lambda_1,\lambda_2}\Big\{&|V_3(\lambda,\lambda_1,-\lambda_2)|^2\left[(1+n_\lambda)(1+n_{\lambda_1})n_{\lambda_2} - n_\lambda n_{\lambda_1}(1+n_{\lambda_2})\right]\delta(\omega_\lambda+\omega_{\lambda_1} \\ &-\omega_{\lambda_2})\delta_{\boldsymbol{q}+\boldsymbol{q}_1,\boldsymbol{q}_2+\boldsymbol{G}} \\ &+\frac{1}{2}|V_3(\lambda,-\lambda_1,-\lambda_2)|^2\left[(1+n_\lambda)n_{\lambda_1}n_{\lambda_2} - n_\lambda(1+n_{\lambda_1})(1+n_{\lambda_2})\right]\delta(\omega_\lambda-\omega_{\lambda_1} \\ &-\omega_{\lambda_2})\delta_{\boldsymbol{q}-\boldsymbol{q}_1,\boldsymbol{q}_2+\boldsymbol{G}}\Big\} \qquad (S3)\end{aligned}$$

$$\left(\frac{\partial n_\lambda}{\partial t}\right)_{4ph} = \frac{2\pi}{\hbar^2}\sum_{\lambda_1,\lambda_2}\Big\{\frac{1}{2}|V_4(\lambda,\lambda_1,\lambda_2,-\lambda_3)|^2\big[(1+n_\lambda)(1+n_{\lambda_1})(1+n_{\lambda_2})n_{\lambda_3}$$
$$- n_\lambda n_{\lambda_1} n_{\lambda_2}(1+n_{\lambda_3})\big]\delta(\omega_\lambda+\omega_{\lambda_1}+\omega_{\lambda_2}-\omega_{\lambda_3})\delta_{\boldsymbol{q}+\boldsymbol{q}_1+\boldsymbol{q}_2,\boldsymbol{q}_3+\boldsymbol{G}}$$
$$+\frac{1}{2}|V_4(\lambda,\lambda_1,-\lambda_2,-\lambda_3)|^2\big[(1+n_\lambda)(1+n_{\lambda_1})n_{\lambda_2}n_{\lambda_3} - n_\lambda n_{\lambda_1}(1+n_{\lambda_2})(1+n_{\lambda_3})\big]\delta(\omega_\lambda$$
$$+\omega_{\lambda_1}-\omega_{\lambda_2}-\omega_{\lambda_3})\delta_{\boldsymbol{q}+\boldsymbol{q}_1-\boldsymbol{q}_2,\boldsymbol{q}_3+\boldsymbol{G}}$$
$$+\frac{1}{6}|V_4(\lambda,-\lambda_1,-\lambda_2,-\lambda_3)|^2\big[(1+n_\lambda)n_{\lambda_1}n_{\lambda_2}n_{\lambda_3}$$
$$- n_\lambda(1+n_{\lambda_1})(1+n_{\lambda_2})(1+n_{\lambda_3})\big]\delta(\omega_\lambda-\omega_{\lambda_1}-\omega_{\lambda_2}-\omega_{\lambda_3})\delta_{\boldsymbol{q}-\boldsymbol{q}_1-\boldsymbol{q}_2,\boldsymbol{q}_3+\boldsymbol{G}}\Big\} \qquad (S4)$$

where

$$V_n(\lambda_1;\dots;\lambda_n) = \left(\frac{\hbar}{2}\right)^{\frac{n}{2}}\frac{\Phi(\lambda_1;\dots;\lambda_n)}{\sqrt{\omega_{\lambda_1}\dots\omega_{\lambda_n}}} \qquad (S5)$$

$$\Phi(\lambda_1;\dots;\lambda_n) = N^{1-\frac{n}{2}}\sum_{\{b,\mu\}}\frac{e_{\mu_1}(b_1;\lambda_1)\dots e_{\mu_n}(b_n;\lambda_n)}{\sqrt{M_{b_1}\dots M_{b_n}}}\sum_{l_2,\dots,l_n}\Phi_{\mu_1\dots\mu_n}(0b_1;l_2b_2;\dots;l_nb_n)$$
$$\times\exp\big[i(\boldsymbol{q}_2\cdot\boldsymbol{r}(l_2)+\dots+\boldsymbol{q}_n\cdot\boldsymbol{r}(l_n))\big] \qquad (S6)$$

Here, $\Phi(\lambda_1;\dots;\lambda_n)$ is the reciprocal space *n*th-order IFCs. $\Phi_{\mu_1\dots\mu_n}(0b_1;l_2b_2;\dots;l_nb_n)$ is the real space *n*th-order IFCs among the atoms $\{b_i\}$ in the cells $\{l_i\}$ along orientations $\{\mu_i\}$ $(i=1,\dots,n)$. M_{b_i} is the mass of atom b_i $(i=1,\dots,n)$. $\boldsymbol{e}(b_i;\lambda)$ is the eigenvector of atom b_i $(i=1,\dots,n)$ at phonon mode λ. Note that permutation symmetry and crystal symmetry are strictly enforced to $V_n(\lambda_1;\dots;\lambda_n)$ in our calculation.

In phonon system, the heat flux is resulted from the deviational distribution function from equilibrium given as $n_\lambda^d = n_\lambda - n_\lambda^0$. At a small ∇T, we consider a small deviation from equilibrium ($n_\lambda^d \ll n_\lambda^0$), which gives the linearized form of Boltzmann transport equation,

$$\boldsymbol{v}_\lambda\cdot\nabla T\frac{\partial n_\lambda^0}{\partial T} = \sum_{\lambda'}A_{\lambda,\lambda'}n_{\lambda'}^d \qquad (S7)$$

where $A_{\lambda,\lambda'}$ is the scattering matrix that quantifies the transition rate from λ' to λ, which can be obtained by linearizing $\left(\frac{\partial n_\lambda}{\partial t}\right)_{3ph}$ and $\left(\frac{\partial n_\lambda}{\partial t}\right)_{4ph}$,

$$\left(\frac{\partial n_\lambda}{\partial t}\right)_{3ph} = \frac{\pi}{\hbar^2}\left\{\sum_{j,k}\left[\left(n^0_{\lambda_2}-n^0_{\lambda_1}\right)n^d_\lambda + \left(n^0_{\lambda_2}-n^0_i\right)n^d_{\lambda_1} + \left(n^0_\lambda + n^0_{\lambda_1}+1\right)n^d_{\lambda_2}\right]W_{\mathrm{I}}^{\lambda,\lambda_1,\lambda_2}\right.$$
$$\left. -\sum_{j,k}\left[\left(n^0_{\lambda_1}+n^0_{\lambda_2}+1\right)n^d_\lambda + \left(n^0_\lambda - n^0_{\lambda_2}\right)n^d_{\lambda_1} + \left(n^0_\lambda - n^0_{\lambda_1}\right)n^d_{\lambda_2}\right]W_{\mathrm{II}}^{\lambda,\lambda_1,\lambda_2}\right\} \quad (S8)$$

$$\begin{cases} W_{\mathrm{I}}^{\lambda,\lambda_1,\lambda_2} = 2|V_3(\lambda,\lambda_1,-\lambda_2)|^2\delta\left(\omega_\lambda+\omega_{\lambda_1}-\omega_{\lambda_2}\right), \text{where } \boldsymbol{q}_2 = \boldsymbol{q}+\boldsymbol{q}_1+\boldsymbol{G} \\ W_{\mathrm{II}}^{\lambda,\lambda_1,\lambda_2} = |V_3(\lambda,-\lambda_1,-\lambda_2)|^2\delta\left(\omega_\lambda-\omega_{\lambda_1}-\omega_{\lambda_2}\right), \text{where } \boldsymbol{q}_2 = \boldsymbol{q}-\boldsymbol{q}_1+\boldsymbol{G} \end{cases} \quad (S9)$$

$$\left(\frac{\partial n_\lambda}{\partial t}\right)_{4ph} = \frac{\pi}{\hbar^2}\left\{\sum_{jkl}\left[-\frac{\left(1+n^0_{\lambda_1}\right)\left(1+n^0_{\lambda_2}\right)n^0_{\lambda_3}}{n^0_\lambda}n^d_\lambda - \frac{\left(1+n^0_\lambda\right)\left(1+n^0_{\lambda_2}\right)n^0_{\lambda_3}}{n^0_{\lambda_1}}n^d_{\lambda_1} - \frac{\left(1+n^0_\lambda\right)\left(1+n^0_{\lambda_1}\right)n^0_{\lambda_3}}{n^0_{\lambda_2}}n^d_{\lambda_2}\right.\right.$$
$$\left. + \frac{\left(1+n^0_\lambda\right)\left(1+n^0_{\lambda_1}\right)\left(1+n^0_{\lambda_2}\right)}{1+n^0_{\lambda_3}}n^d_{\lambda_3}\right]W_{\mathrm{III}}^{\lambda,\lambda_1,\lambda_2,\lambda_3}$$
$$+\sum_{jkl}\left[-\frac{\left(1+n^0_{\lambda_1}\right)n^0_{\lambda_2}n^0_{\lambda_3}}{n^0_\lambda}n^d_\lambda - \frac{\left(1+n^0_\lambda\right)n^0_{\lambda_2}n^0_{\lambda_3}}{n^0_{\lambda_1}}n^d_{\lambda_1} + \frac{\left(1+n^0_\lambda\right)\left(1+n^0_{\lambda_1}\right)n^0_{\lambda_3}}{1+n^0_{\lambda_2}}n^d_{\lambda_2}\right.$$
$$\left. + \frac{\left(1+n^0_\lambda\right)\left(1+n^0_{\lambda_1}\right)n^0_{\lambda_2}}{1+n^0_{\lambda_3}}n^d_{\lambda_3}\right]W_{\mathrm{IV}}^{\lambda,\lambda_1,\lambda_2,\lambda_3}$$
$$+\sum_{jkl}\left[-\frac{n^0_{\lambda_1}n^0_{\lambda_2}n^0_{\lambda_3}}{n^0_\lambda}n^d_\lambda + \frac{\left(1+n^0_\lambda\right)n^0_{\lambda_2}n^0_{\lambda_3}}{1+n^0_{\lambda_1}}n^d_{\lambda_1} + \frac{\left(1+n^0_\lambda\right)n^0_{\lambda_1}n^0_{\lambda_3}}{1+n^0_{\lambda_2}}n^d_{\lambda_2}\right.$$
$$\left.\left. + \frac{\left(1+n^0_\lambda\right)n^0_{\lambda_1}n^0_{\lambda_2}}{1+n^0_{\lambda_3}}n^d_{\lambda_3}\right]W_{\mathrm{V}}^{\lambda,\lambda_1,\lambda_2,\lambda_3}\right\} \quad (S10)$$

$$\begin{cases} W_{\mathrm{III}}^{\lambda,\lambda_1,\lambda_2,\lambda_3} = |V_4(\lambda,\lambda_1,\lambda_2,-\lambda_3)|^2\delta\left(\omega_\lambda+\omega_{\lambda_1}+\omega_{\lambda_2}-\omega_{\lambda_3}\right), \text{where } \boldsymbol{q}_3 = \boldsymbol{q}+\boldsymbol{q}_1+\boldsymbol{q}_2+\boldsymbol{G} \\ W_{\mathrm{IV}}^{\lambda,\lambda_1,\lambda_2,\lambda_3} = |V_4(\lambda,\lambda_1,-\lambda_2,-\lambda_3)|^2\delta\left(\omega_\lambda+\omega_{\lambda_1}-\omega_{\lambda_2}-\omega_{\lambda_3}\right), \text{where } \boldsymbol{q}_3 = \boldsymbol{q}+\boldsymbol{q}_1-\boldsymbol{q}_2+\boldsymbol{G} \\ W_{\mathrm{V}}^{\lambda,\lambda_1,\lambda_2,\lambda_3} = \frac{1}{3}|V_4(\lambda,-\lambda_1,-\lambda_2,-\lambda_3)|^2\delta\left(\omega_\lambda-\omega_{\lambda_1}-\omega_{\lambda_2}-\omega_{\lambda_3}\right), \text{where } \boldsymbol{q}_3 = \boldsymbol{q}-\boldsymbol{q}_1-\boldsymbol{q}_2+\boldsymbol{G} \end{cases} \quad (S11)$$

Considering a linear expansion of n_λ with respect to ∇T, $n_\lambda^d = \left(-\partial n_\lambda^0/\partial T\right)\mathbf{F}_\lambda \cdot \nabla T$, where the expansion coefficient $\mathbf{F}_\lambda$ can be obtained by solving the linearized Boltzmann transport equation through self-consistent iteration. Since the heat flux $J^\alpha = \frac{1}{N}\sum_\lambda \hbar\omega_\lambda v_\lambda^\alpha n_\lambda^d = -\kappa^{\alpha\beta}\nabla_\beta T$ the lattice thermal conductivity can be derived from

$$\kappa^{\alpha\beta} = \frac{1}{N}\sum_\lambda C_\lambda v_\lambda^\alpha F_\lambda^\beta \qquad (S12)$$

where α and β denotes the crystal directions and $\lambda \equiv (\boldsymbol{q}, p)$ labels a phonon mode with wave vector $\boldsymbol{q}$ and polarization p. C_λ and v_λ^α is the volumetric specific heat and the group velocity along α direction of phonon mode λ, respectively. *N* is the number of $\boldsymbol{q}$-points in the mesh of the Brillouin Zone.

S3. Comparison of temperature dependent thermal conductivity of *R3m*-BNC_2 vs. BAs.

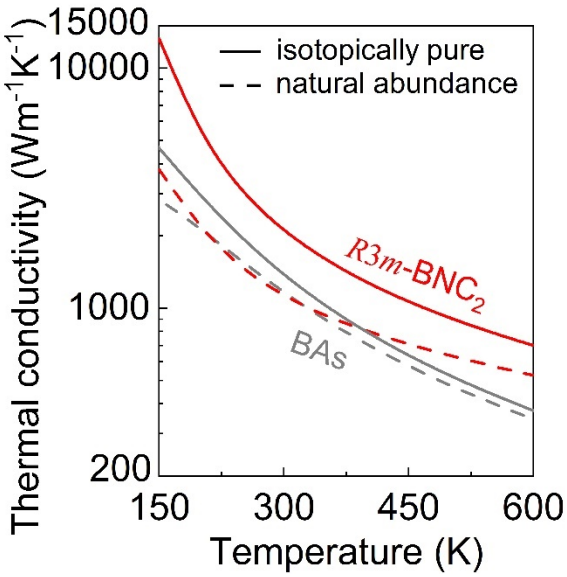

Figure S1. Thermal conductivity of *R3m*-BNC_2 vs. BAs, considering both isotopically pure and naturally occurring isotope concentrations.

S4. Comparison between RTA and iterative solution of thermal conductivity.

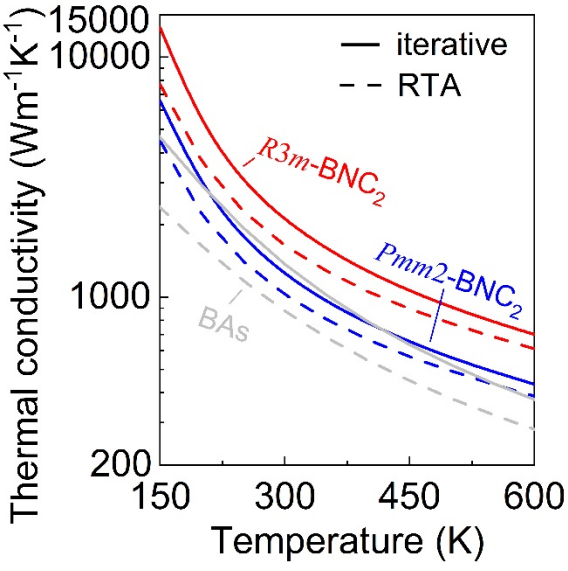

Figure S2. RTA vs iterative solution of thermal conductivity.

S5. Comparison of phonon mean free path spectra calculated with and without four-phonon process.

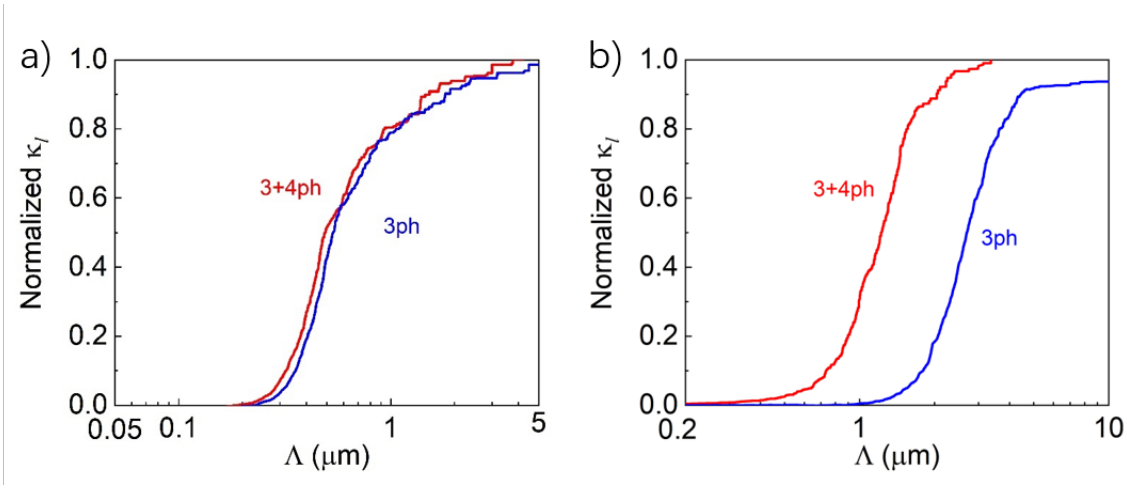

Figure S3. Phonon mean free path distributions calculated with and without 4-phonon scattering for (a) *R3m*-BNC_2 and (b) BAs. 3ph indicates the calculation with only 3-phonon process and 3+4ph indicates the calculation with both 3 and 4 phonon processes.

S6. Details in crystal structure.

We calculated BNC_2 of different *R3m*, *Pmm2*, and $P\bar{4}m2$ phases using primitive cells with four atoms. The primitive cells for different phases are shown in Figure S3. The first Brillouin zone for different phases are shown in Figure S4.

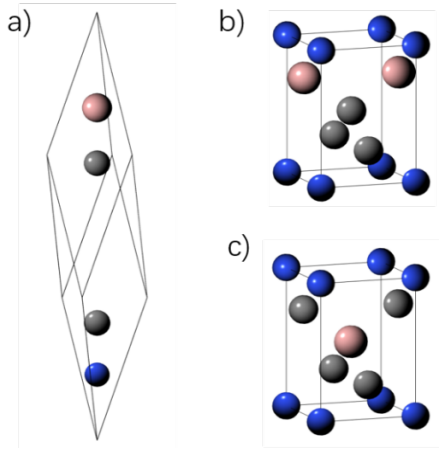

Figure S4. Primitive cell of (a) *R3m*-BNC_2, (b) *Pmm2*-BNC_2 and (c) $P\bar{4}m2$ -BNC_2. The pink, gray and blue spheres indicate boron, carbon, and nitrogen atoms respectively.

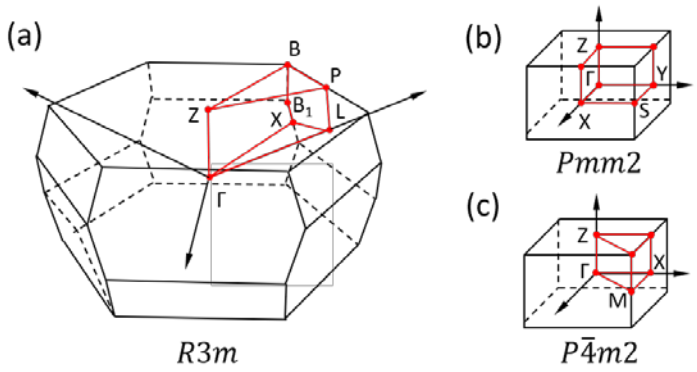

Figure S5. First Brillouin zone of (a) *R3m*, (b) *Pmm2*, and (c) $P\bar{4}m2$ phases of BNC_2.

S7. Electronic band gap

We calculated the electronic structure of *R3m*, *Pmm2*, and $P\bar{4}m2$ phases of BNC_2 based on density functional theory using Heyd-Scuseria-Ernzerhof screened hybrid functional [8] with SG15 Optimized Norm-Conserving Vanderbilt pseudopotentials [9]. We used 12×12×12 Monkhorst-Pack grid and 6×6×6 mesh for the sampling of the Fock operator. The kinetic energy cutoff for wavefunctions is 120 Ry. The convergence of all the setting has been carefully checked. We found that *R3m*-BNC_2 has a wide bandgap at 5.1 eV. And the calculated electronic band gap for *Pmm*2 and $P\bar{4}m2$ are 2.9 eV and 3.2eV, respectively.

References:

[1] P. G. and S. B. and N. B. and M. C. and R. C. and C. C. and D. C. and G. L. C. and M. C. and I. D. and A. D. C. and S. de G. and S. F. Wentzcovitch, J. Phys. Condens. Matter **21**, 395502 (2009).

[2] P. G. and O. A. and T. B. and O. B. and M. B. N. and M. C. and R. C. and C. C. and D. C. and M. C. and N. C. and I. C. and A. D. C. and S. de G. and P. D. and R. A. D. J. and A. Baroni, J. Phys. Condens. Matter **29**, 465901 (2017).

[3] T. Tadano, Y. Gohda, and S. Tsuneyuki, J. Phys. Condens. Matter **26**, 225402 (2014).

[4] We used the pseudopotentials B.pz-n-kjpaw_psl.0.1.UPF, C.pz-n-kjpaw_psl.0.1.UPF, N.pz-n-kjpaw_psl.0.1.UPF, P.pz-n-kjpaw_psl.0.1.UPF, As.pz-n-kjpaw_psl.0.2.UPF, and Si.pz-n-kjpaw_psl.0.1.UPF from the Quantum ESPRESSO pseudopotential data base: http://www.quantum-espresso.org/pseudopotentials. .

[5] Y. Wang, J. J. Wang, W. Y. Wang, Z. G. Mei, S. L. Shang, L. Q. Chen, and Z. K. Liu, J. Phys. Condens. Matter **22**, 202201 (2010).

[6] P. E. Blöchl, O. Jepsen, and O. K. Andersen, Phys. Rev. B **49**, 16223 (1994).

[7] G. P. Srivastava, *The Physics of Phonons* (CRC Press, 1990).

[8] J. Heyd, G. E. Scuseria, and M. Ernzerhof, J. Chem. Phys. **118**, 8207 (2003).

[9] D. R. Hamann, Phys. Rev. B **88**, 085117 (2013).